Accepted manuscript doi:
10.1680/jmacr.18.00441

Accepted manuscript doi:
10.1680/jmacr.18.00441

Submitted: 14 September 2018

Published online in 'accepted manuscript' format: 14 February 2019

Manuscript title: Exposed Aggregate Areas and Photocatalytic Efficiency of Photocatalytic Aggregate Mortar

Authors: L. Zheng[1], M. R. Jones[1], L. Yang[2], A. Hakki[2] and D. E. MacPhee[2]

Affiliations: [1]Division of Civil Engineering, University of Dundee, Dundee, DD1 4HN, Scotland, UK and [2]Department of Chemistry, University of Aberdeen, Aberdeen, AB24 3UE, Scotland, UK

Corresponding author: L. Zheng, Division of Civil Engineering, University of Dundee, Dundee, DD1 4HN, Scotland, UK. Tel.: +44 1382 384723; Fax: +44 1382 384389.

E-mail: l.zheng@dundee.ac.uk

Accepted manuscript doi:
10.1680/jmacr.18.00441

Abstract

Having the potential to remove NOx air pollutants, generated by vehicles and other anthropogenic combustion processes particularly in urban areas, photocatalytic concrete has attracted significant commercial interests all over the world. In contrast to typical photocatalyst applications in concrete, in which TiO_2, the most utilised photocatalyst, is dispersed within the cementitious materials, the study reported here utilises TiO_2-coated aggregates. Used in an exposed aggregate finish, this format aims to have a higher photocatalytic efficiency than TiO_2 – cement bound materials. An exposed TiO_2-coated aggregate has the potential to provide a significant higher proportion of catalyst to direct UV radiation and to minimise performance lost due to occlusion. The surface area on the aggregate exposed on the test mortar samples was measured with 3D imaging techniques. Thereafter, photocatalytic efficiency was measured in comparison with that of the TiO_2 cement mortar. The relationship between exposed area for photocatalytic reaction and photocatalytic efficiency was established. This indicated that the photonic efficiency increases with increasing exposed area, regardless of the method to support the catalyst, i.e. either within the cement paste or externally mounted on the aggregate. The data confirm that exposing coated aggregate significantly enhances photonic efficiency.

Keywords: Aggregates; Mortar; Testing, apparatus & methods; TiO_2 Coated Aggregate; Exposed Surface Area; Photocatalytic Efficiency

Accepted manuscript doi:
10.1680/jmacr.18.00441

1. Introduction

'Photocatalytic concrete' has attracted significant interest all over the world as it has the potential to remove pollutants generated by vehicles and combustion, such as NOx, aromatics, ammonia and aldehydes from the atmospheres (e.g. Cassar, 2004; Hanus and Harris, 2013). TiO_2, in the form of anatase, is the most widely used photocatalyst, due to its strong oxidizing power under near-UV radiation and its chemical stability in concrete. TiO_2 is typically incorporated by intermixing with the cementitious phase and then applied to the surfaces of buildings (walls and roofs), roads and footpaths, etc. to create reactive surfaces (Ballari, et al, 2010). It has been demonstrated that pollutants, at concentrations typically ranging from 0.01ppm to 10ppm, which are typical of highway tunnels, can be reduced by the deployment of photocatalytic concrete (Fujishima, et al, 2008).

Most current applications utilise a coating or a thin cementitious layer where the photocatalyst is added as a powder or a suspension (Dylla, et al, 2011). While the surface layering method results in a larger proportion of the TiO_2 being exposed to solar radiation, this format is susceptible to loss of the catalyst from environmental abrasion (Diamanti, et al, 2008; Ramirez, et al, 2010). Alternatively, it can be intermixed with cement and made into concrete elements. These are more durable but photocatalytic activity is significantly degraded due to a large amount of the TiO_2 being occluded. The presence of ionic species in cement also reduces the photocatalytic efficiency due to the charge recombination (Rachel, et al, 2002). A further problem is the tendency of TiO_2 particles to agglomerate in the cement paste, which reduces the effective TiO_2 surface area for photocatalytic activity.

In the research reported here, a novel method to support the TiO_2 catalyst is described in which the particles are bonded to quartz sand that is then applied to the surface of the fresh concrete as an exposed aggregate. Given the high cost of the catalyst the aim was to maximise the exposed surface area whilst minimising any losses from the deployed concrete units. A schematic comparison of the conventional and novel methods to support the catalyst is shown in Figure 1.

For this new system, the available photocatalyst surface area on the aggregates and their bound strength to the mortar substrate are then the key factors to affect the performance efficiency and durability. As the exposed surface area of the aggregate was particular difficult to evaluate from these aggregate exposed mortar samples, 3D imaging with μCT scanner was developed for this purpose. Test to determine the ability of this system to oxidise NOx was then carried out to establish the underpinning relationship between exposed area and photocatalytic performance.

2. Experimental Details

2.1 Materials

The following materials were used to produce TiO_2 coated aggregate and aggregate exposed mortar for testing.

- TiO_2 powder additive PC105, a commercially available anatase.
- Standard quartz sand conforming to BS EN 196-1 (BSI, 2005).
- CEM I 52,5N (PC) conforming to BS EN 197-1 (BSI, 2011).

Accepted manuscript doi:
10.1680/jmacr.18.00441

2.2 Preparation of TiO_2 Coated Aggregate

The sand was sieved on a 1mm sieve and the retained material (1-2mm) was used as the catalyst support. Note it was assumed that this size range would be the easiest to bond to the cementitious substrate while providing the largest exposed surface area.

The TiO_2 aggregate coating process followed the method previously described by Lu, et al (2017) and the key stage are summarised here. Firstly, a TiO_2 hydrosol suspension was prepared from a low-temperature precipitation-peptization process (Burunkaya, et al, 2013; Li, et al, 2014). Secondly, the quartz sand particles were added into the suspension with the pH value controlled to 13±0.1 using a 1M NaOH solution. The mixture was then stirred for 48 hours at room temperature allowing the TiO_2 to chemically bond to the surface of the sand. The solution was drained and the product was washed with 25% ethanol-water solution to neutral pH and oven dried at 105°C for 24 hours.

The chemical compositions of the test materials are given in Table 1.

X-ray fluorescence spectroscopy (XRF) showed that the coated sand had a TiO_2 loading of 0.34%. XRD analysis showed only quartz peaks and an anatase content below the limit of detection.

2.3 Preparation of Exposed Aggregate Mortar

The preparation of the base mortar followed the method described in BS EN 196-1 (BSI, 2005). Mortar samples with an as-cast surface area size of 100×50 mm and thickness of 15 mm were prepared. This size allowed the samples to be place in a photocatalytic performance test reactor conforming to ISO 22197−1 (ISO, 2016). Actual sample exposed surface area was 99×50mm due to the 2mm thickness PMMA plate to separate the samples in the cast mould (Figure 2a). The process to prepare the aggregate exposed mortar was as follows:

(i) Pre-laying aggregates on 50mm wide self-adhesive tape: to ensure specific amount of single layer aggregate was mounted to each test sample the coated sand was pre-laid on to a 99mm long adhesive tape, the mass of which was recorded. Typically, this enabled around 9 to 10g of the coated sand to be mounted. The tape was weighed to obtain the exact mass that had been deployed.

(ii) Sample casting: 200×50×50mm moulds were used and a 2mm PMMA separator plate was used to produce two 99mm long test samples, as shown schematically in Figure 2a. PU foam (density = 40kg/m^3) was used to give the required 15mm thickness. After casting, the aggregate-coated tape was then placed on to the freshly as-cast surface of the mortar substrate and pressed into the surface under the load of a concrete block with different weight (Figure 2b) to give the specified aggregate exposure (via the depth of embedment). The samples were demoulded after 24 hours and standard cured in water for 7 days. The tapes were then peeled off from the hardened mortar, leaving one layer of aggregates exposed on the top surface of the samples.

Accepted manuscript doi:
10.1680/jmacr.18.00441

Two levels aggregate 'exposure' were tested, i.e. 1/3 and 2/3 nominal exposure height (or 2/3 and 1/3 embedment) respectively. There were some losses during the tape peeling process, i.e. some aggregate particles remained adhered to the tape after peeling, with more in 2/3 than in 1/3 exposure samples. Consequently, the peeled tape was weighed after deposition to determine the amount of aggregates that had been actually attached to each test sample.

For comparison, conventional intermixed TiO_2 – cement mortar reference samples were also prepared. The TiO_2 – cement was prepared by adding 5% anatase TiO_2 powder (PC105) by mass into the PC during mortar mixing. The mix proportion of the mortar was the same as BS EN 196-1 standard mortar. Once prepared, a 2 mm thick layer of the mortar mixture was applied to the top of the pre-made mortar substrate.

2.4 Test Methodologies

Measurement of exposed aggregate surface area

Enumerating the 3-dimensional exposed surface area of the coated aggregates is difficult and few methods have been published (Panda, et al, 2016). The estimation of specific surface of particles traditionally is based on their size distribution curve and assuming a spherical shape for the particles (McCabe et al., 2005). To improve the accuracy for natural aggregates, modified methods have been proposed assuming angular solid shapes (e.g. Ghasemi, et al, 2018) or by considering elongation and flakiness parameters (e.g. Panda, et al, 2016). Other models use empirical surface area factors (e.g. Hmoud, 2011).

3D laser scanning methods have also been used (e.g. Alshibli, et al, 2015; Garboczi and Bullard, 2017), but their use is limited due to high equipment costs (or low resolution) and problems with shadows affect its accuracy. As a result, 3D laser scanning has only been used for coarse aggregates (e.g. Anochie-Boateng et al. 2011; Asahina and Taylor, 2011).

To counter these issues a novel technique was developed in this study using 3D Computerised micro-tomography (µCT) image analysis. Scans of the test samples were obtained with Nikon XT H 225 ST and reconstructed by using proprietary software (VG STUDIO 3.1, Volume Graphics GmbH, 2017). These scans had a linear resolution of 0.056 mm. Higher resolutions were possible but only be reducing the sample size and thus affecting the representativeness of the test sample.

Distinguishing exposed aggregates from the underlying base mortar by X-ray tomography was also challenging. This was mainly due to the densities of the aggregate and cement materials being similar and thus difficult to distinguish by µCT. To overcome this problem, a reference sample was made using a known amount of aggregate applied to a PMMA plate and its 3D CT scanned image to calibrate the measurement of exposed aggregate area for different exposure heights. This produced 3D CT scan images in which the test sand could be distinguished easily from underlying PMMA base.

The reference sample was made from a 100×50×2mm PMMA plate, applying a film of adhesive on one surface, then, the aggregates were affixed in the same way as that used to prepare the sand-tape. The sand covered area was 90×50mm (10mm at one end was used to clip the sample to the sample table of the CT scanner). The weight of the adhered sand was recorded as 6.578g.

Accepted manuscript doi:
10.1680/jmacr.18.00441

In the current study, only the overall exposed surface area of the object was calculated directly. This contrasts with previous work (e.g. Jia and Garboczi, 2016; Garboczi and Bullard, 2017) where a set of individual particles was measured, characterised and then modelled. The approach allows additional physical parameters to be calculated, such as particle size distribution and various shape parameters, i.e. elongation and flakiness, et al. for the purpose of digital simulation of concrete mixture. However, it could have a problem in surface area calculation in this study since the surfaces of modelled particles could be 'smoothed' during the modelling process and then the surface area underestimated.

Photocatalytic performance

Photocatalytic performance of the test samples was measured using a flow-through reactor as described by Lu, et al (2017) and illustrated schematically in Figure 3.

The test sample was placed inside the reactor to enable the laminar flow of NO gas over the sample surface. The sample was irradiated with a 500W Xe-lamp solar illuminator (Sciencetech. Inc) light source. A 1000 ppb NO concentration at 40% RH, as measured using a HygroPalm 1 detector (Rotronic) at 25°C, was passed over the test sample at a volumetric flow rate of 5×10^{-5} m^3/s. The concentrations of NO, NO_2 and NOx were measured using a Thermo Scientific Model 42i-HL High Level NO-NO_2-NOx Analyzer (Air Monitors Ltd). Each test sample firstly remained in the reactor but under dark conditions until equilibrium concentrations were reached (around 30 min) and subsequently, under illumination, until steady state concentrations were observed (around 2 hrs). The resulting photon flux at the position of the sample was measured to be 3.05×10^{-5} $mol/s\cdot m^2$ using a broadband thermopile detector (Gentec-EO-XLP12-3S-H2-D0). For comparison, the photocatalytic performances of uncoated sand mortar and photocatalyst intermixed with cement mortar samples were measured under identical conditions. The photocatalytic efficiency ($\boldsymbol{\xi}$) and the catalyst selectivity for nitrate ($\boldsymbol{S}$ %) were calculated according to Equations (1) and (2) respectively.

$$\xi = \frac{(c_d - c_i)VP}{\phi ART} \quad (1)$$

$$S = \frac{\xi_{NOx}}{\xi_{NO}} \quad (2)$$

where $\boldsymbol{c_d}$ is the concentration in the dark, $\boldsymbol{c_i}$ the concentration under illumination, $\boldsymbol{V}$ the volumetric flow rate, $\boldsymbol{P}$ the pressure, $\boldsymbol{A}$ the irradiated sample area, $\boldsymbol{R}$ the gas constant, $\boldsymbol{T}$ the absolute temperature, and $\boldsymbol{\Phi}$ the photon flux impinging the photocatalyst surface. The photocatalytic efficiency was determined separately for *NO*, NO_2, and total *NOx*.

3. Results and Discussion

3.1 Calculated Exposed Surface Area

Surface area of aggregates adhered to the PMMA plate

Figure 4 shows example images of the sample of aggregates attached to the PMMA plate. Figure 4a shows a conventional digital photo and Figure 4b the histogram of the reconstructed 3D CT image. There are three distinguishing peaks in the histogram representing air, PMMA plate and sand respectively. Figures 4c and 4d show the reconstructed images with and without PMMA plate respectively. Total aggregate surface area, S_{totol}, was then calculated using Figure 4d, on which only aggregates are shown and the PMMA plate been filtered out.

Accepted manuscript doi:
10.1680/jmacr.18.00441

To calculate the exposed aggregate surface area a set of 'regions of interest' (ROIs) were selected, as shown in Figure 5. The ROIs were rectangular prisms, covering the top and side planes, with the bottom plane considered varying distances from the aggregate coated surface of the PMMA plate. Figure 5a shows the intersection of the bottom plane and the aggregates, which intersects the aggregates and divided them into two parts:

(i) The upper part represents the aggregates that would be embedded into the mortar, which is within the ROI. The surface area of aggregates in this part represents the bound area between exposed aggregates and mortar substrate, S_{bound}, and the intersection area, $S_{intersection}$, can be calculated.

(ii) The lower part represents the aggregates to be exposed to the air after peeling. The surface area of aggregates in this part, representing exposed aggregate surface areas, $S_{exposed}$, can be derived by

$$S_{exposed} = S_{totol} - S_{bound} \quad (3)$$

As illustrated in Figure 5, the distance between the PMMA plate surface and the digital 'cut surface' of the ROI represents the aggregate exposure height in the mortar samples.

Figure 6 shows the calculated exposed aggregate area varying with the aggregate exposure height. The bound area follows the same curve, however, the values are given in the right axis and the values for embedment depth given in the top axis. A line for the global sample upper surface area (around 90 × 50mm), which equates to the surface area of the reference mortar sample is also shown. As expected the exposed aggregate area increased with increasing aggregate exposure height. When it reaches 1/3 exposure height, the aggregate exposure area approaches the same as the global sample surface area. Increasing exposure height further results in the aggregate exposure area being higher than the global sample surface area, which provides a greater surface area for photocatalytic activity, as illustrated in Figure 1. Above a 2/3 exposure height, the increase in exposure area was limited. Indeed, in practice it decreases since the smallest particles do not adhere to the mortar surface. Therefore, the maximum practical exposure height for aggregates is around 2/3.

The area of the interaction of the ROI 'cut surface' and aggregates is also calculated and its varying with aggregate exposure height is shown in Figure 6. The intersection area increases with the aggregate exposure height to a maximum point, which is just beyond the 1/3 exposure height, and then decreases with further increasing aggregate exposure height. When 2D photos are taken from the top view, the intersection should be the same as the projected area of the exposed aggregate. However, the 'real' intersection is hidden under the shadow of this maximum intersection.

If the particles were ideal, i.e. spherical and in uniform 2 mm size, the intersection curve would be symmetrical with the maximum point in the middle of the exposure height/embedment depth. However, in practice, aggregates are irregular particles and in this case with sizes ranging from 1-2 mm (Figure 4). Smaller particles tended to lodge near to the PMMA plate surface and on the mortar substrate tended to be exposed on the top surface. Thus, the maximum point moved to a deeper embedment depth, i.e. less exposure height.

Accepted manuscript doi:
10.1680/jmacr.18.00441

Given larger exposed areas results in a lower bound area, a balance has to be struck between maximising the potential photocatalytic performance and the aggregate retention on the substrate. In addition, the results shown in Figure 5 are affected by the spacing of the aggregates on the mortar surface. The results shown in Figure 5 were obtained with 6.578g sand mounted on to a 90.33×51.02 mm plate surface, i.e. the aggregate distribution density = 1.427kg/m^2. It is reasonable to assume that the exposed area is proportional to the distribution density within a certain range, however, further work is required to confirm this.

It should also be noted that Figure 5 shows that particles also agglomerated, i.e. areas not shown as blue and it is likely that this reduces photocatalytic performance slightly due to particles 'shadowing' each other.

Exposed surface area of aggregates on mortar samples

Four test mortar samples, two each for 1/3 and 2/3 nominal aggregate exposure heights respectively, were prepared using the method described in Section 2. As mentioned in Section 2.3, some aggregates were lost during the tape application process. The level of exposed aggregates remaining on the base mortar surface was recorded (Table 2) and was dependent on the exposure height/embedment depth. An initial quantity of around 9g sand was applied to the tape. The total sand loss was 16.7% for 1/3 exposure height samples and 33.1% for 2/3 exposure height. This resulted in lower aggregate distribution density in 2/3 exposure height samples (1.249 kg/m^2) than that in 1/3 exposure height samples (1.538 kg/m^2). The aggregate distribution density for PMMA plate was targeted in between them with the value of 1.427 kg/m^2 for the purpose to estimate the exposed areas of mortar samples.

An example of the aggregate exposed mortar for CT scan test is shown in Figure 7, where Figure 7a is the digital photo and Figure 7b the reconstructed 3D image from the CT scan.

The exposed aggregate area calculation was similar to that for the PMMA plate sample. A set of ROIs were selected, as shown in Figure 8. The regions were rectangular prisms, covering the top plane with varying depths. The differences from the PMMA plate sample were that:

(i) The side faces of the sample (around 5 mm) were digitally 'cut' as the uneven top surface was observed at the near edge area. An 80×40 mm global area was selected in the middle of the sample as ROI, as shown in Figures 9a-9c.

(ii) The histogram of the CT reconstructed 3D image (shown in Figure 8d) indicates that the exposed aggregates and the base mortar could not be separated. Therefore, the area determined with CT scanning data is the total area of exposed aggregates and the actual exposed surface area was, therefore, difficult to determine.

In the selected ROIs, two area values can be calculated: (i) total exposed area, which includes both exposed aggregates and top mortar surface uncovered by the exposed aggregates, and (ii) total intersections of ROI and mortar sample at bottom and side. Since the surface to embed exposed aggregates is the as-cast surface, the surface is rough, therefore, the exposure depth has a small range of variation.

Accepted manuscript doi:
10.1680/jmacr.18.00441

Figure 9 illustrates the approach developed to determine the exposure height of the aggregates and hence derive the aggregate exposed surface area. Two curves, i.e. total surface area and total intersection, plotted against the ROI height are shown in Figure 9a. By adjusting the intersection of the bottom plane of the ROI it eventually coincides with the mortar substrate, as schematically shown in Figure 9b where: P_1 = the lowest aggregate exposure height, P_2 = the highest aggregate exposure height, and P_3 = the surface of the mortar substrate. The estimated aggregate exposure area is then determined on the corresponding total surface area curve with P_1 and P_2.

Figure 10 illustrates the different ROI heights with Figures 10b, c and d showing views at P_1, P_2 and P_3 respectively. These intersection images were also used to cross check the estimated P_1, P_2 and P_3 points.

Using the same approach, the exposures height and exposed area of all samples were calculated, as given in Figure 11. As the global sample surface was 99×50 mm (= 4950 mm^2) but the ROI 80×40mm, a factor of 1.55 [= (99×50)/(80×40)] was applied. The calculated surface areas of exposed aggregates ranged from 5892 to 7539 mm^2.

Due to the size variation of the aggregates, controlling the actual depth of 'penetration' into the substrate mortar was difficult. While the 2/3 exposed aggregate height control came close to the target i.e. 1.33 mm, the 1/3 height control tended to be more exposed than intended i.e. 0.67 mm, and was nearer to ½ height exposed. Given this there was a lower aggregate loss during the sample preparation, Table 2, than that of 2/3 exposed aggregate sample, the real total exposed surface area of 1/3 exposed aggregate sample was not reduced with increasing embedding (i.e. reducing exposure height) in the range tested as shown in the figure.

The surface area of exposed aggregate, based on results from the PMMA plate sample, was also estimated with the results shown in Figure 11. These data are an overestimation, since there was no aggregate loss, which happened during the tape-based application of the exposed aggregate mortar samples. The value given from PMMA sample represents the up-limits of the exposed aggregate area for the mortar samples and this gives a cross check of the calculation.

3.2 Photocatalytic Performance

Photocatalytic performance was measured on the four mortar samples with one reference TiO_2 – cement mortar and the results of which are given in Figure 12. Compared to reference TiO_2 – cement mortar, photocatalyst-treated aggregate samples have significantly increased photonic efficiency.

The relationship between photonic efficiency and the exposed area of aggregate is plotted in Figure 13 and demonstrates the advantage of this form. This relationship holds regardless of how TiO_2 is supported, either in the cement paste or aggregate mounted.

4. Practical Implications

In comparison to the incorporation of the TiO_2 catalyst directly into the paste phase, surface mounting on to aggregate exposed mortars resulted in a higher photocatalytic efficiency due to an enhances area of catalysis per unit weight of material. This is important as anatase TiO_2 is an expensive material (note it is not possible to provide costs in this paper as these are

commercial-in-confidence with manufacturers). However, it is estimated that given the increased photocatalytic efficiency of external mounting the amount of anatase required per unit surface area can be reduced to about 1/20 of that of the conventional method of intermixing with the paste phase, which could bring significant cost reduction for photocatalytic concrete production.

5. Conclusions

The research reported proposes a novel way of supporting TiO_2 photocatalyst by chemically bonding them to aggregates that are then mounted as an exposed aggregate. It is demonstrated that this achieves a higher photocatalytic efficiency when compared to the convention process of mixing with cement. Enumerating the surface area exposed was problematic but using digital manipulation of μCT scanned images it was possible quantitatively measure the surface area of treated aggregate, although its application can only be undertaken in small-scale laboratory test samples. The test also indicate that an improvement is needed in the application of treated aggregates as the losses due to adhesive-based aggregate mounting method were around 33% and 17% for the 2/3 and 1/3 exposure areas respectively.

Acknowledgements

The authors gratefully acknowledge funding from the UK Engineering and Physical Sciences Research Council (Grant EP/M003299/1) and the Natural Science Foundation of China (Grant 51461135005) International Joint Research Project (EPSRC-NSFC). Thanks are also given to Mr. Anthon Tacussel Da Silva, Mr. Victor Leger, Mr. Robim Campos and Miss Axelle Airmard for their samples preparation and early exploring studies and to Dr. Laszlo Csetenyi for his help in CT scanning.

List of Notation

- $\boldsymbol{\xi}$ photocatalytic efficiency, %
- $\boldsymbol{\Phi}$ photon flux impinging the photocatalyst surface, mol/s·m^2
- $\boldsymbol{c_i}$ concentration under illumination, %
- $\boldsymbol{c_d}$ concentration in the dark, %
- $\boldsymbol{A}$ irradiated sample area, m^2
- $\boldsymbol{P}$ pressure, bar
- $\boldsymbol{R}$ gas constant, J/molK
- $\boldsymbol{S}$ catalyst selectivity for nitrate, %
- S_{bound} bound area between exposed aggregates and mortar substrate, mm^2
- $S_{exposed}$ exposed aggregate surface areas, mm^2
- $S_{intersection}$ intersection area, mm^2
- S_{totol} total aggregate surface area, mm^2
- $\boldsymbol{T}$ absolute temperature, K
- $\boldsymbol{V}$ volumetric flow rate, m^3/s

Accepted manuscript doi:
10.1680/jmacr.18.00441

References

Alshibli KA, Druckrey AM, Al-Raoush RI, Weiskittel T and Lavrik NV (2015) Quantifying morphology of sands using 3D imaging. *Journal of Materials in Civil Engineering, ASCE*, **27(10)**: 04014275.

Anochie-Boateng J, Komba J and Tutumluer E (2011) 3D laser based measurement of mineral aggregate surface area for South African hot mix asphalt mixtures. In: *90th Annual Meeting of Transport Research Board*, Washington DC, 2011.

Asahina D and Taylor MA (2011) Geometry of irregular particles: Direct surface measurements by 3-D laser scanner. *Powder Technology*, **213(1/3)**: 70–78.

Ballari MM, Hunger M, Hüsken G and Brouwers HJH (2010) Modelling and experimental study of the NOx photocatalytic degradation employing concrete pavement with tutanium dioxide. *Catalysis Today*, **151(1/2)**: 71–76.

BSI (British Standards Institution) (2005) BS EN 196-1:2005. Methods of testing cement. Part 1: Determination of strength. BSI, London, UK.

BSI (British Standards Institution) (2011) BS EN 197-1:2011. Cement. Part 1: Composition, specifications and conformity criteria for common cements. BSI, London, UK.

Burunkaya E, Akarsu M, Erdem Çamurlu H, Kesmez Ö, Yeşil Z, Asiltürk M and Arpaç E (2013) Production of stable hydrosols of crystalline TiO_2 nanoparticles synthesized at relatively low temperatures in diverse media. *Applied Surface Science*, **265**: 317−323.

Cassar L (2004) Photocatalysis of cementitious materials: Clean buildings and clean air. *MRS Bulletin*, **29(5)**: 328−331.

Diamanti MV, Ormellese M and Pedeferri MP (2008) Characterization of photocatalytic and superhydrophilic properties of mortars containing titanium dioxide. *Cement and Concrete Research*, **38(11)**: 1349-1353.

Dylla H, Hassan MM, Schmitt M, Rupnow T, Mohammad LN and Wright E (2011) Effects of roadway contaminants on titanium dioxide photodegradation of nitrogen oxides. *Transportation Research Record*; **2240**: 22–29.

Fujishima A, Zhang X and Tyrk DA (2008) TiO_2 photocatalysis and related surface phenomena. *Surface Science Reports*, **63(12)**: 515–582.

Garboczi EJ and Bullard JW (2017) 3D analytical mathematical models of random star-shape particles via a combination of X-ray computed microtomography and spherical harmonic analysis. *Advanced Powder Technology*, **28(2)**: 325–339.

Ghasemi Y, Emborg M and Cwirzen A (2018) Estimation of specific surface area of particles based on size distribution curve. *Magazine of Concrete Research*, **70(10)**: 533–540.

Jia X and Garboczib EJ (2016) Advances in shape measurement in the digital world. *Particuology*, **26**: 19–31

Hanus MJ and Harris AT (2013) Nanotechnology innovations for the construction industry. *Progress in Materials Science*, **58(7)**: 1056–1102.

Hmoud HR (2011) Evaluation of VMA and film thickness requirements in Hot-Mix Asphalt, *Modern Applied Science*, **5(4)**: 166 – 176.

ISO (International Organization for Standardization) (2016). ISO 22197-1:2016 Fine ceramics (advanced ceramics, advanced technical ceramics) — Test method for air-purification performance of semiconducting photocatalytic materials — Part 1: Removal of nitric oxide. ISO, Geneva, Switzerland.

Li Y, Qin Z, Guo H, Yang H, Zhang G, Ji S and Zeng T (2014) Low-temperature synthesis of anatase TiO_2 nanoparticles with tunable surface charges for enhancing photocatalytic activity. *PLoS One*, **9(12)**: e114638.

Lu Y, Hakki A, Wang F and MacPhee DE (2017) Different Roles of Water in Photocatalytic DeNOx Mechanisms on TiO_2: Basis for Engineering Nitrate Selectivity? *ACS Applied Materials & Interfaces*, **9(20)**: 17034–17041

McCabe WL, Smith JC and Harriott P (2005) Unit Operations of Chemical Engineering, 7th Ed, McGraw-Hill, New York, 1140p.

Panda RP, Das SS and Sahoo PK (2016) An empirical method for estimating surface area of aggregates in hot mix asphalt, *Journal of Traffic and Transportation Engineering (English edition)*, **3(2)**: 127 – 136

Rachel A, Subrahmanyam M and Boule P (2002) Comparison of photocatalytic efficiencies of TiO_2 in suspended and immobilized form for the photocatalytic degradation of nitrodenzenesulfonic acids. *Applied Catalysis B: Environmental*, **37(4)**: 301-308.

Ramirez AM, Demeestere K, De Belie N, Mantyla T and Levanen E (2010) Titanium dioxide coated cementitious materials for air purifying purposes: preparation, characterisation and toluene removal potential. *Building and Environment*, **45(4)**: 832-838.

Volume Graphics GmbH (2017) VG STUDIO Max 3.1 Reference Manual, Volume Graphics GmbH, 69115 Heidelberg, Germany.

Accepted manuscript doi:
10.1680/jmacr.18.00441

Table captions

Table 1 Chemical composition of PC and aggregates used in this study

Table 2 Exposed aggregates remaining on the sample and their distribution density

Table 1 Chemical composition of PC and aggregates used in this study

Test Material	Chemical composition, % by mass									
	CaO	SiO_2	Al_2O_3	Fe_2O_3	MgO	MnO	TiO_2	K_2O	Na_2O	SO_3
PC (CEM I)	60.39	18.64	4.33	2.66	1.03	0.04	0.22	0.62	0.43	4.65
Quartz Sand	0.29	89.42	0.49	0.07	0.04	-	0.02	0.03	0.04	0.08
TiO_2 Coated Quartz Sand	0.04	89.06	0.37	0.09	0.02	-	0.36	0.02	0.08	0.02

Table 2 Exposed aggregates remaining on the sample and their distribution density

Sample Code	Nominal Exposure Height	Aggregate Mass, g		Total Loss, %	Global Sample Surface Area, mm^2	Aggregate Distribution Density, kg/m^2
		Initial	Remained at CT scan and photocatalytic performance test			
Perspex plate	-	6.578	-	-	4609	1.427
Mortar STA-2/3-1	2/3 1.33 mm	9.100	6.206	31.80	4950	1.254
Mortar STA-2/3-2		9.400	6.158	34.49	4950	1.244
Mortar STA-1/3-1	1/3 0.67 mm	9.230	7.700	16.58	4950	1.556
Mortar STA-1/3-2		9.050	7.530	16.80	4950	1.521

Accepted manuscript doi:
10.1680/jmacr.18.00441

Figures captions

Figure 1 Schematic comparison of the two techniques for application of TiO_2 photocatalysts in concrete: (a) intermixed TiO_2 - cement layer and (b) exposed aggregate mortar

Figure 2 Casting mortar samples: (a) schematic of the samples in a $200\times50\times50mm^2$ mould; (b) laying exposed aggregate tape on fresh cast sample with a controlled pressure.

Figure 3 Photocatalytic performance test setup

Figure 4 Test sample of aggregates mounted on PMMA plate. (a) Photo; (b) Histogram of the CT reconstructed 3D image; (c) CT reconstructed 3D image; (d) CT reconstructed 3D image, with PMMA plate been filtered out;

Figure 5 Selection of region of interest (ROI) on the sample: (a) Intersection of the bottom plane and the aggregates; (b) Side view and determination of the aggregate exposure height

Figure 6 Aggregate exposed area varying with aggregate exposure height/embedment depth

Figure 7 Sample of exposed aggregates mortar (Sample: Mortar STA-2/3-1). (a) Photo; (b) CT reconstructed 3D image

Figure 8 The sample of aggregates sticking on mortar substrate (Sample: Mortar STA-2/3-1). (a) Bottom view; (b) Long side view; (c) Short side view; (d) Histogram

Figure 9 The approach to estimate the exposure height and surface area of exposed aggregates (Sample: Mortar STA-2/3-1): (a) total surface area and intersection varying with ROI height; and (b) schematic illustration points of P_1, P_2 and P_3.

Figure 10 Bottom intersection at different ROI heights (Sample: Mortar STA-2/3-1). (a) Height = 0; (b) Height = 1.1 mm (P_1); (c) Height = 1.4 mm (P_2); (d) Height = 2.0 mm (P_3)

Figure 11 The exposed area of aggregate in mortar samples and their exposure height

Figure 12 Performance of the photocatalyst-treated exposed aggregate mortar

Figure 13 Relationship between photonic efficiency and exposed area for photocatalytic reaction

Accepted manuscript doi:
10.1680/jmacr.18.00441

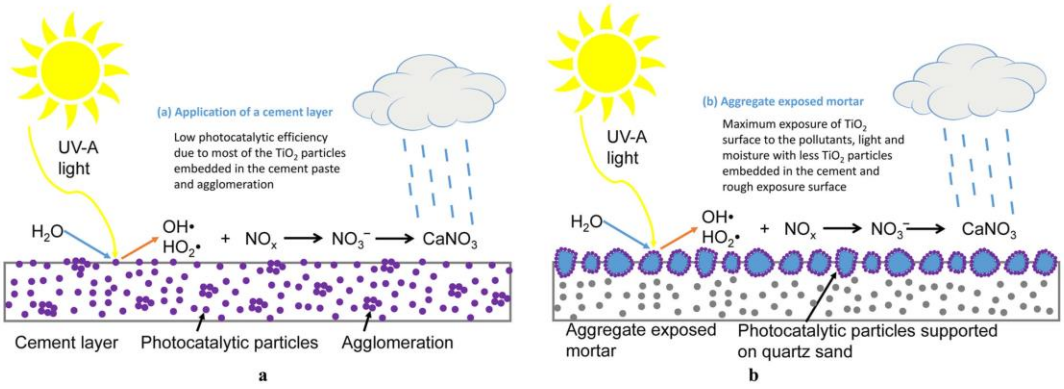

Figure 1

Accepted manuscript doi:
10.1680/jmacr.18.00441

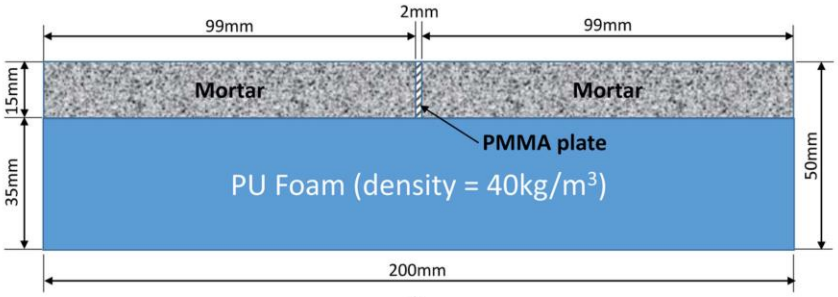

a

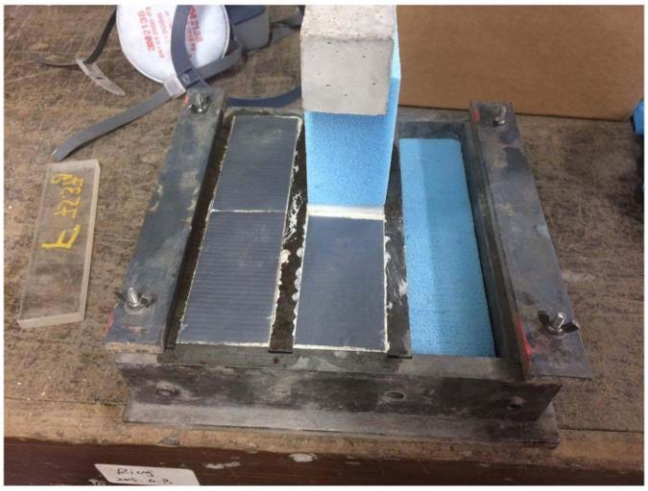

b

Figure 2

Accepted manuscript doi:
10.1680/jmacr.18.00441

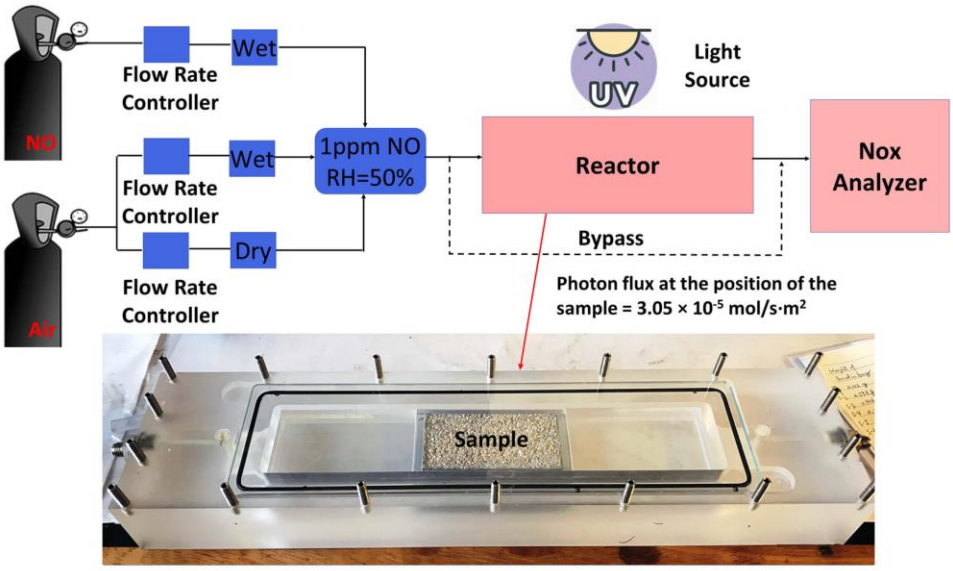

Figure 3

Accepted manuscript doi:
10.1680/jmacr.18.00441

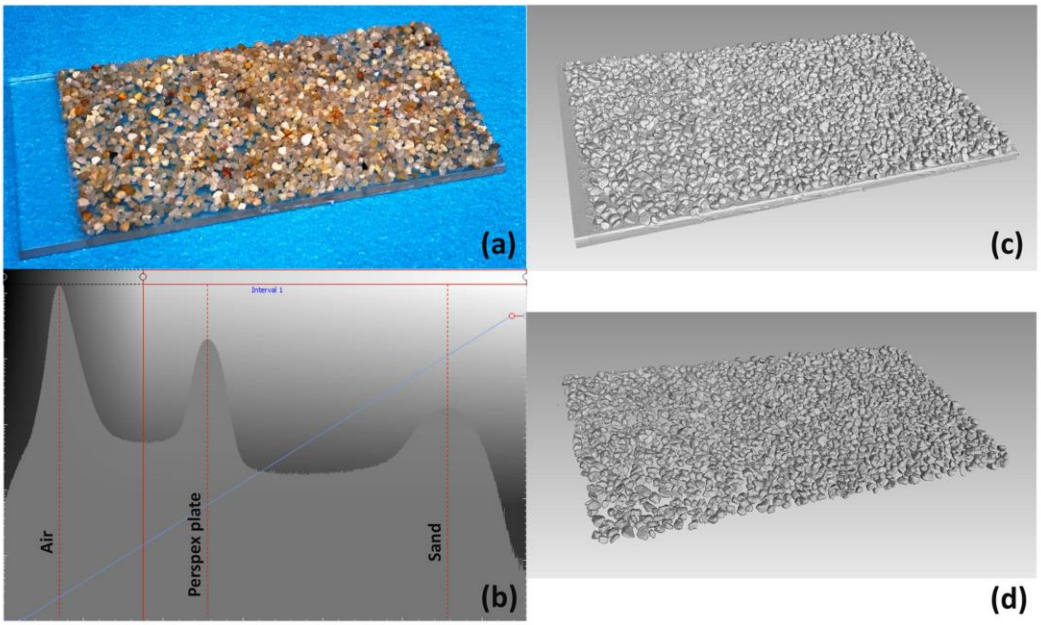

Figure 4

Accepted manuscript doi:
10.1680/jmacr.18.00441

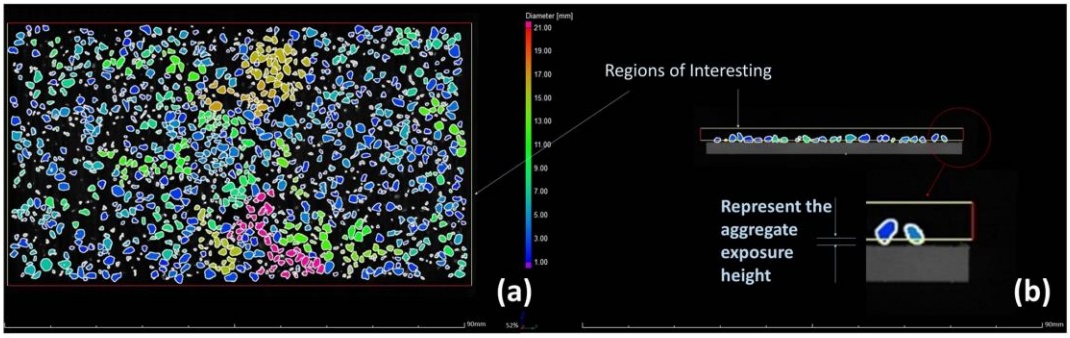

Figure 5

Accepted manuscript doi:
10.1680/jmacr.18.00441

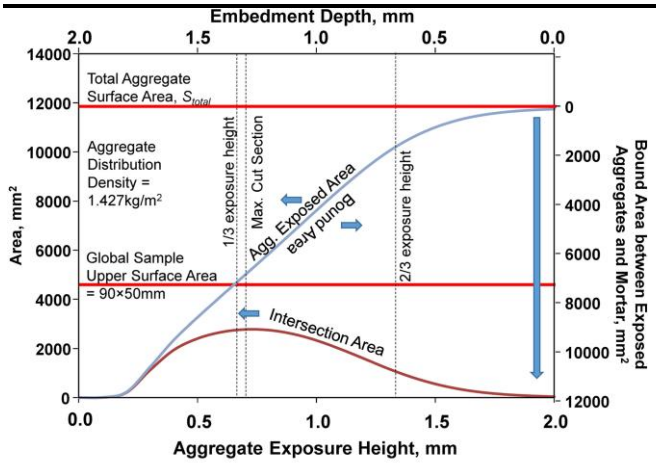

Figure 6

Accepted manuscript doi:
10.1680/jmacr.18.00441

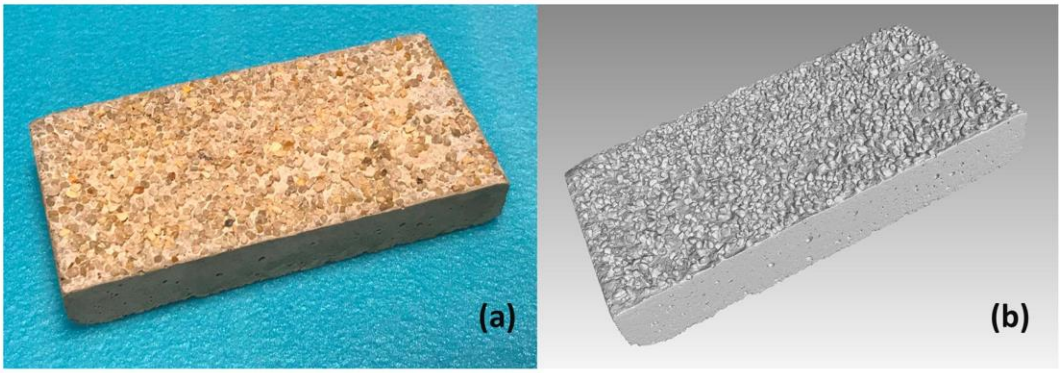

Figure 7

Accepted manuscript doi:
10.1680/jmacr.18.00441

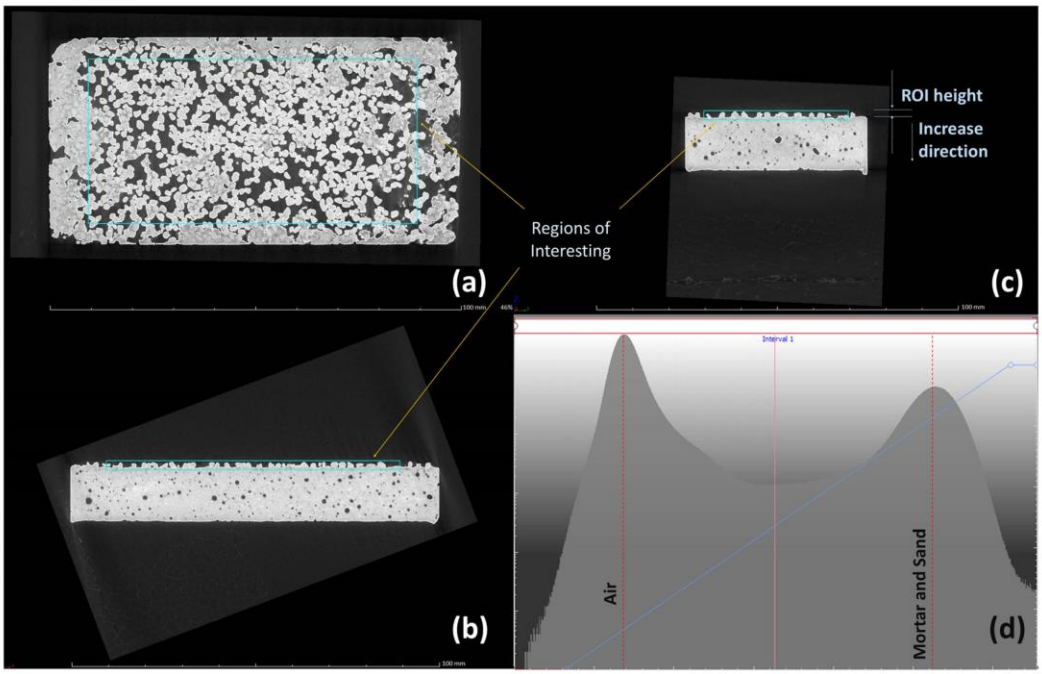

Figure 8

Accepted manuscript doi:
10.1680/jmacr.18.00441

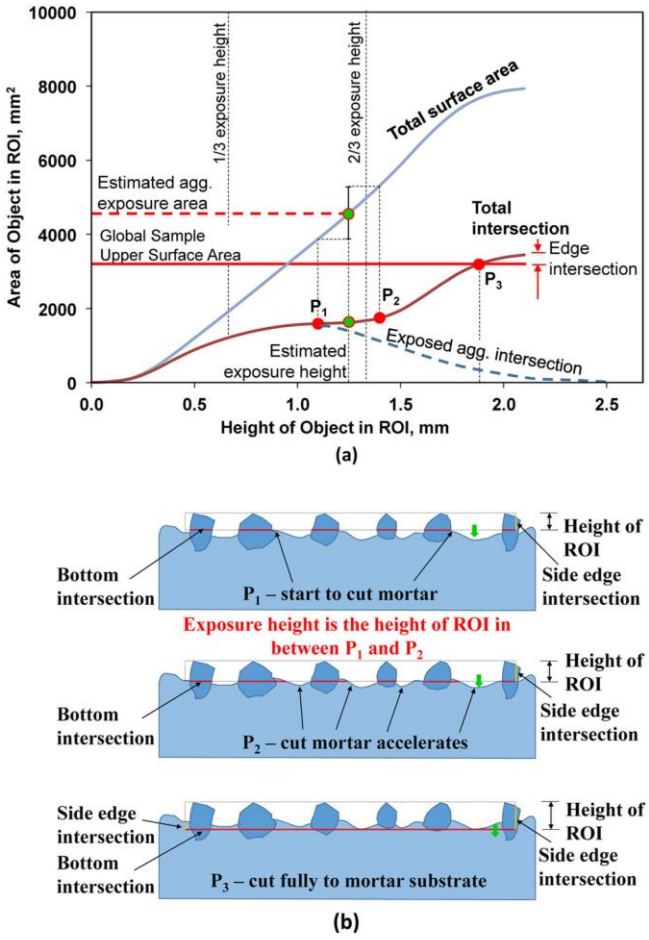

Figure 9

Accepted manuscript doi:
10.1680/jmacr.18.00441

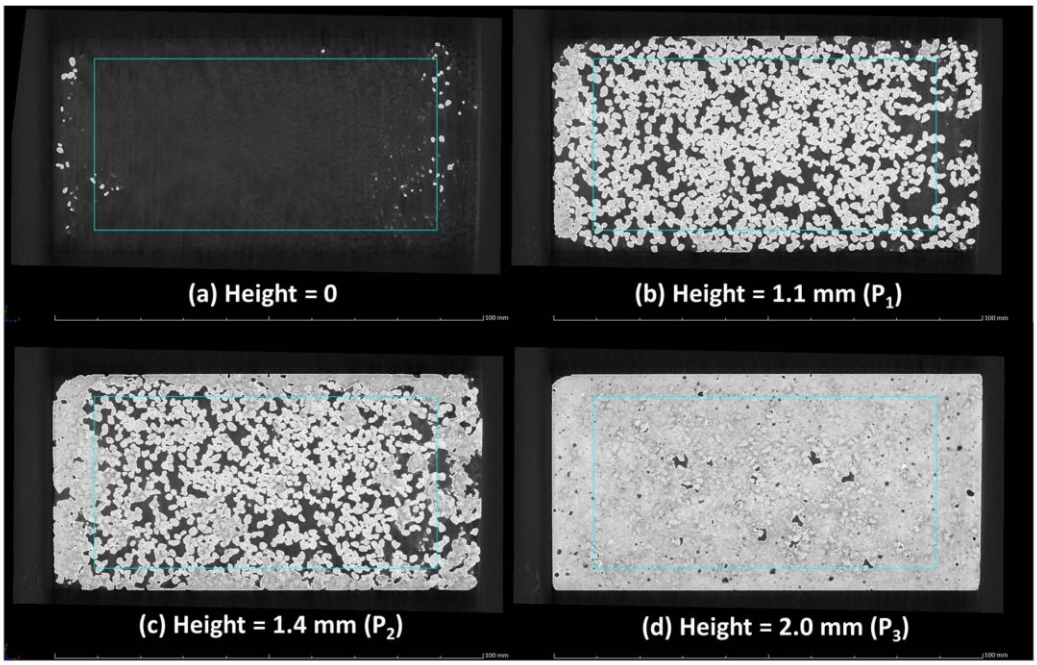

Figure 10

Accepted manuscript doi:
10.1680/jmacr.18.00441

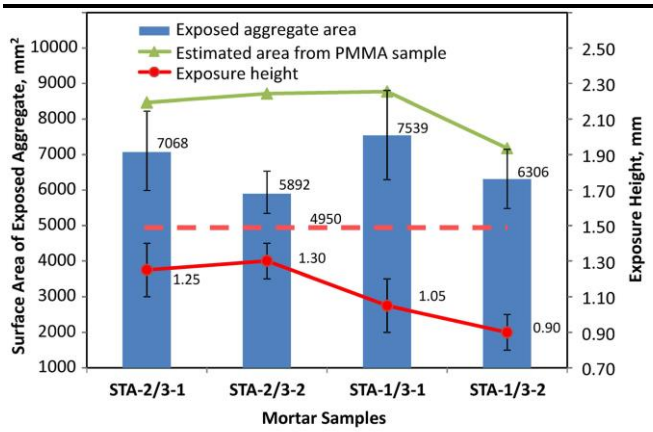

Figure 11

Accepted manuscript doi:
10.1680/jmacr.18.00441

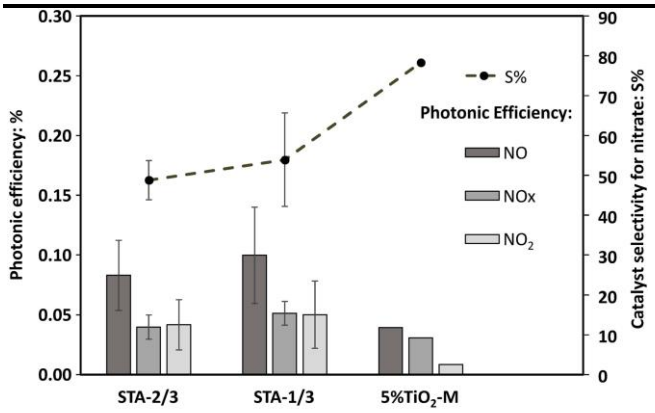

Figure 12

Accepted manuscript doi:
10.1680/jmacr.18.00441

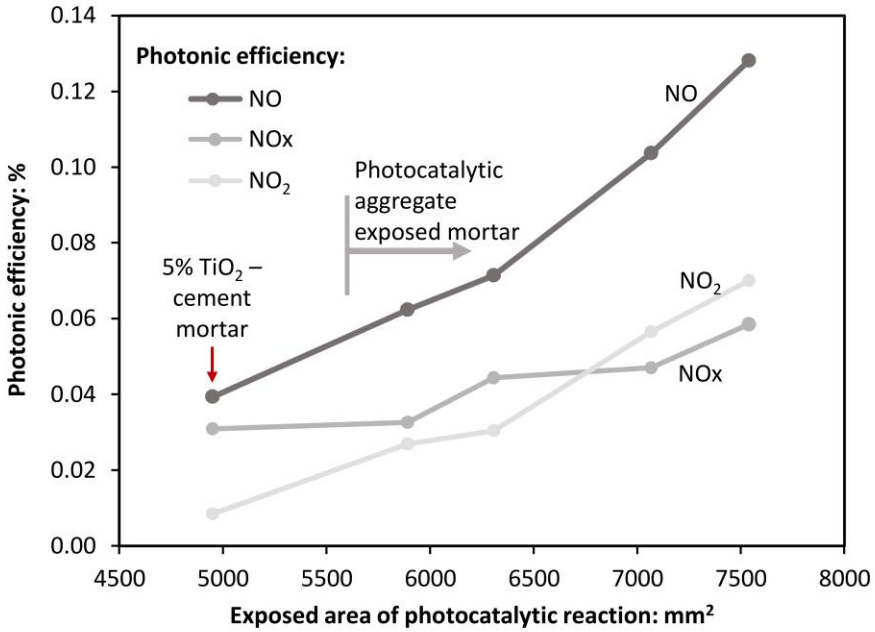

Figure 13